Modelling of linear motor end-effects for saliency based sensorless control

Modelling of linear motor end-effects for saliency based sensorless control

P. Giangrande, F. Cupertino
Politecnico di Bari
Via Orabona, 4
Bari 70125, Italy

G. Pellegrino
Politecnico di Torino
C.so Duca degli Abruzzi, 24
Torino 10129, Italy

E-mail: giangrande@deemail.poliba.it

Abstract -- **In linear motors, the open structure of the armature produces the so called end-effect. The end-effect introduces non-idealities in the motor magnetic model in dq-synchronous coordinates that require a specific modelling with respect to the well known models of rotating (cylindrical) machines. In particular, for saliency based sensorless control, the end-effect introduces an error in the estimated position that must be taken into account and properly compensated. This paper introduces a general mathematical modeling of the end-effect that can be applied to all linear machines. Based on such model, modified position observers are proposed for sensorless control using pulsating or rotating voltage vectors. Experimental results are presented to verify the feasibility of the proposed method, with reference to the case of a linear tubular permanent magnet motor.**

***Index Terms*—Permanent magnet linear synchronous motor, end-effect, mathematical model, sensorless control.**

I. INTRODUCTION

Nowadays there is an increasing demand for linear motion in several industrial and robotic applications. Hence linear motor drives are widely used in applications such as pick and place, X-Y machines, linear compressors, elevator doors and industrial robots [1,2]. The linear motors offer many advantages compared to those based on the traditional rotating motors: the elimination of the transmission gears (zero backlash), the simplification of the construction and the reduction of the maintenance. In addition, with the advent of the high-energy rare-earth permanent magnets, the linear motors allow obtaining high force-to-volume ratios and high drive performance [3].

Linear motor technology offers many configurations, with their advantages and disadvantages, and among the commonly used structures for linear permanent magnet synchronous motors (LPMSMs) the tubular one allows to better exploit the permanent magnet flux reducing size and end effects.

In particular, the tubular LPMSM is constituted by an armature containing the three phase windings and a rod containing the permanent magnets [4]. The rod can be internal or external with respect to the armature and both topologies could be either moving rod or moving armature. The armature can be air-cored or iron-cored and in the latter case it could be slotted or slotless.

The topology considered in this work is described in figure 1. It has an inner rod and a moving armature, iron cored and slotless. The magnets inside are axially magnetized and enclosed into a stainless steel tube (not represented in the figure). Such PM rods give a good performance and can be manufactured easily with much lower cost with respect to rods with radial magnetization. The adjacent PMs of opposite polarities are spaced by ferromagnetic disks (iron spacers). The main functions of the stainless steel shield are supporting and protecting the permanent magnets and pole-pieces [2]. Such configuration is referred as internal permanent magnet (IPM) and presents magnetic saliency [5] that makes the motor suitable for sensorless position control based on signal injection [6-8].

In the recent years, several papers have been published about the analysis, modelling and compensation of the end-effect [9,10], but few of them have considered its impact on the sensorless control techniques. In this paper, an end-effect analysis is presented and its main contribution is in the modeling of the end-effect in terms of high-frequency magnetic model of the linear motor, that is the one to be considered for injection based sensorless control strategies.

The end-effect, due to the open structure of the armature, results in a position estimation error when standard sensorless techniques are applied, since such techniques are valid for rotating motors that have no end-effect. In other words, the end-effect error must be modeled with the aim of compensating the related position tracking error.

A high-frequency mathematical model of the linear motor is introduced, where the end-effects are taken into account. An effective method to compensate the impact of the end-effect on position sensorless control is also presented.

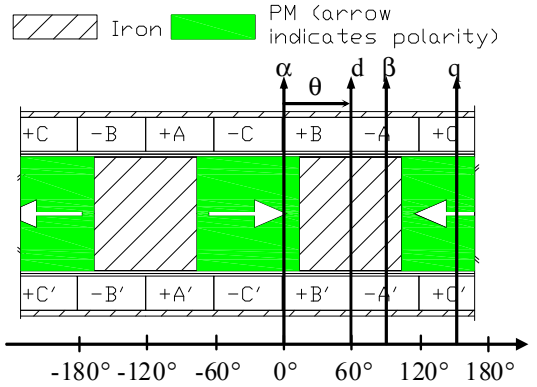

Fig. 1 Section of the IPM tubular motor and definition of the reference axis and relative position of rod and armature θ in electrical degrees.

II. Linear Motor Structure and End-Effect

In this work we consider three-phase linear actuators of the tubular topology but the proposed model is of general validity for all linear motors. The tubular motor structure is represented in figure 1, where the stationary (α-β) and synchronous (d-q) reference frames are defined together with the electrical position θ. The three-phase windings are mounted on the moving part and are arranged as *A*-*C*-*B*-*A*-*C*-*B* along the axial direction. The permanent magnets are sintered NdFeB disks. As said, they are axially magnetized and separated by iron spacers.

The general relationship between phase currents and phase linked fluxes for a three-phase motor is expressed by (1). There is no permanent magnet (PM) contribution in (1) because the paper deals with the high-frequency model valid for saliency based sensorless control [11].

$$\boldsymbol{\lambda}_{ABC} = \begin{bmatrix} L_A & M_{AB} & M_{AC} \\ M_{BA} & L_B & M_{BC} \\ M_{CA} & M_{CB} & L_C \end{bmatrix} \cdot \mathbf{i}_{ABC} \tag{1}$$

The self-inductances are indicated with L and the mutual inductances are indicated with M. As usual for salient motors, all the inductances are a function of the position θ.

The motor self and mutual phase inductances at injection frequency have been measured by means of a dedicated test bench according to the scheme of figure 2. Each phase, in turn, was supplied with a sinusoidal voltage signal at 1000 Hz using a Chroma 61703 power supply. The current of the supplied phase and the voltages of the two non supplied phases were measured at different positions of the motor rod using oscilloscope probes (see figure 2). When the phase *A* was supplied, the formulas used to determine L_A, M_{AB} and M_{AC} in each considered motor position were the following (the resistive drops are neglected):

$$\begin{aligned} L_A(\theta) &= \frac{V_{AN}}{\omega_i I_A(\theta)} \\ M_{AB}(\theta) &= \frac{V_{BN}(\theta)}{\omega_i I_A(\theta)} \\ M_{AC}(\theta) &= \frac{V_{CN}(\theta)}{\omega_i I_A(\theta)} \end{aligned} \tag{2}$$

where ω_i is the pulsation of the voltage supply. The test was repeated three times for evaluating the self and mutual inductances of all the motor phases. The measured inductances are reported in figure 3 as function of motor position and expressed in both the ABC and the d-q reference frame. In particular, figure 3a shows the measured self and mutual inductances of the tubular motor under test as a function of the position over an entire electrical period.

The variation of the inductances with the position is at twice the electrical frequency and it is not exactly sinusoidal due to the motor geometry (in particular the PM to iron ratio of the rod). Apart for the non-sinusoidal shape, the three self-inductances have all the same waveform, and they are displaced by one third of their period as it happens for rotating motors [12], independently of the end-effect. On the contrary, the end-effect of the motor under test is evidenced in figure 3a by the M_{AB} mutual term: phases *A* and *B* both have one coil at one of the motor ends and their mutual coupling is generally lower (in absolute value, since mutual inductances are negative) with respect to M_{CA} and M_{BC} terms that both involve phase *C*.

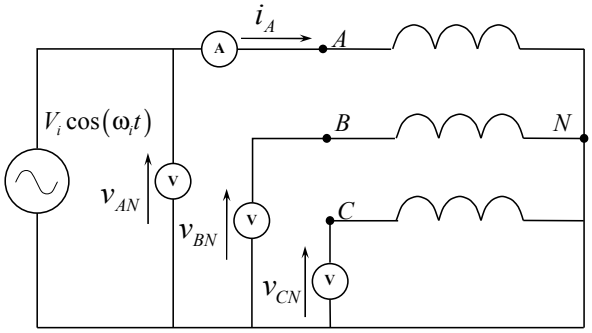

Fig. 2 Scheme used to measure the high frequency inductances.

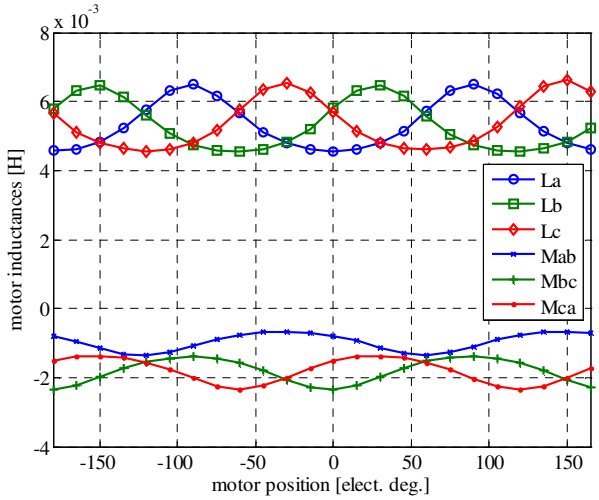

(a)

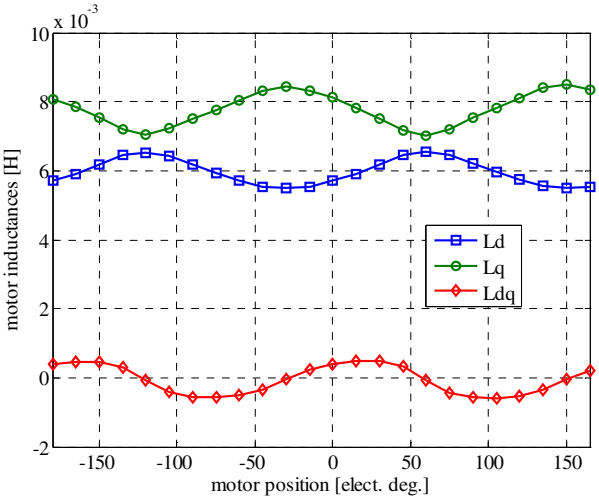

(b)

Fig. 3 Measured motor inductances at 1000 Hz in the *ABC* (a) and d-q (b) reference frame.

This is due to the unsymmetrical distribution of the phase windings, which makes the coupling effect between phase *A* and *B* weaker than that of others. In *d-q* coordinates (figure 3b) the unbalanced mutual inductances produce two effects that will be addressed in the next section:

- the direct and quadrature inductances (L_d, L_q) vary with the position;
- a cross-coupling term (L_{dq}) appears, and it is also a function of the position.

Dealing with sensorless control, the reduction of the motor saliency $L_q - L_d$ under certain positions (e.g. -120° and 60° in figure 3) deteriorates signal to noise ratio of the position tracking. Nevertheless, the most significant impact of end-effect on sensorless control stability is due to the cross-coupling term, that produces an orientation error, as demonstrated in the case of L_{dq} terms given by magnetic saturation [14]. Figure 4 reports the field distribution of the armature of a simplified tubular motor with only 3 coils, one for each phase so to clarify how the end-effect is originated. The field distribution has been obtained by means of finite-element analysis (FEA). In figure 4a only phase *C* is supplied while in figure 4b only phase *A* is supplied with the same DC current value. From figure 4a it is evident that the mutual inductances M_{CB} and M_{CA} are equal, while from figure 4b results that the mutual coupling term M_{AB} is lower with respect to M_{AC} (= M_{CA}.). Practical windings adopt a higher number of coils and this reduces the asymmetry of the mutual inductances. Slotted armatures also mitigate the end-effect that is nevertheless present in linear machines of all kinds and sizes [13].

III. Modelling of the End-Effect

Going back to figure 3b, all the inductance terms vary with the position with a period that is twice the electrical period defined in figure 1. As said, the *A-B* mutual term M_{AB} is different from M_{BC} and M_{CA} due to the end-effect: in particular the alternating part has the same amplitude and shape for all the mutual inductances while the average value of M_{AB} is lower (in absolute values) than the other two mutual terms.

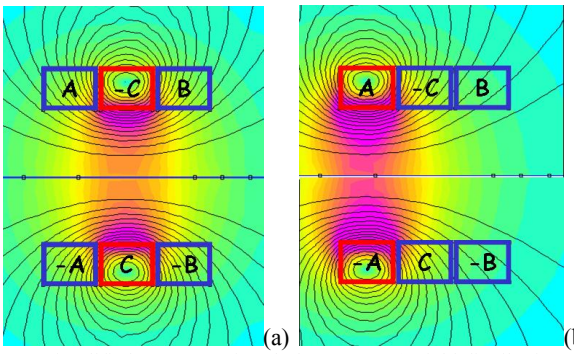

(a) (b)

Fig. 4 Simplified armature of a tubular motor. (a) Field distribution when only phase *C* is supplied. (b) Field distribution when only phase *A* is supplied.

In the following, the simplified sinusoidal model of such effect will be reported (3) and developed. Let M_0 be the average value of M_{AB}, and let M_2 be the amplitude of the alternating components of M_{AB}, M_{BC} and M_{CA}: the two mutual terms that involve phase *C* have an augmented average coupling indicated as ΔM_0. About self inductances let L_0 be the average value of self inductance and let L_2 be the amplitude of the self inductance oscillation. To summarize, the end-effect is modeled in (3) by the term ΔM_0.

$$\begin{cases} L_A = L_0 + L_2\cos(2\vartheta) \\ L_B = L_0 + L_2\cos\left(2\vartheta + \frac{2}{3}\pi\right) \\ L_C = L_0 + L_2\cos\left(2\vartheta - \frac{2}{3}\pi\right) \end{cases} \qquad (3)$$

$$\begin{cases} M_{AB} = M_0 + M_2\cos\left(2\theta - \frac{2}{3}\pi\right) \\ M_{BC} = M_0 + M_2\cos(2\theta) + \Delta M_0 \\ M_{CA} = M_0 + M_2\cos\left(2\theta + \frac{2}{3}\pi\right) + \Delta M_0 \end{cases}$$

Substituting the equation (3) in (1), the high frequency model which includes the end effect's asymmetry has been obtained:

$$\begin{aligned} \boldsymbol{\lambda}_{ABC} = & \left\{ L_0 + L_2 \begin{bmatrix} \cos(2\theta) & 0 & 0 \\ 0 & \cos\left(2\theta + \frac{2}{3}\pi\right) & 0 \\ 0 & 0 & \cos\left(2\theta - \frac{2}{3}\pi\right) \end{bmatrix} \right\} \mathbf{i}_{ABC} + \\ & + M_2 \begin{bmatrix} 0 & \cos\left(2\theta - \frac{2}{3}\pi\right) & \cos\left(2\theta + \frac{2}{3}\pi\right) \\ \cos\left(2\theta - \frac{2}{3}\pi\right) & 0 & \cos(2\theta) \\ \cos\left(2\theta + \frac{2}{3}\pi\right) & \cos(2\theta) & 0 \end{bmatrix} \mathbf{i}_{ABC} + \\ & + M_0 \cdot \begin{bmatrix} 0 & 1 & 1 \\ 1 & 0 & 1 \\ 1 & 1 & 0 \end{bmatrix} \mathbf{i}_{ABC} + \Delta M_0 \begin{bmatrix} 0 & 0 & 1 \\ 0 & 0 & 1 \\ 1 & 1 & 0 \end{bmatrix} \mathbf{i}_{ABC} \end{aligned} \qquad (4)$$

In (4) the first three terms represent the flux linkage due to the self and mutual inductances respectively, while the last term is the amount given by the unbalancing caused by the end-effect. Using the Park transformation, the linear motor model can be express in the reference frame synchronous with motor position as reported in equation (5) at the top of next page. To put in evidence the non idealities introduced in the *dq* model by the end-effect, the linked fluxes are split in two contributions by means of the superposition principle: first the fluxes without the end-effect ($\Delta M_0 = 0$) and then the flux produced by the mutual terms unbalance alone ($\Delta M_0 \neq 0$).

$$\boldsymbol{\lambda}_{dq} = \begin{vmatrix} L_0 + \frac{1}{2}L_2 - M_0 + M_2 + \frac{2}{3}\Delta M_0\left[1-\cos\left(2\theta - \frac{2}{3}\pi\right)\right] & -\frac{2}{3}\Delta M_0 \sin\left(2\theta - \frac{2}{3}\pi\right) \\ -\frac{2}{3}\Delta M_0 \sin\left(2\theta - \frac{2}{3}\pi\right) & L_0 - \frac{1}{2}L_2 - M_0 - M_2 - \frac{2}{3}\Delta M_0\left[\cos\left(2\theta - \frac{2}{3}\pi\right) - 1\right] \end{vmatrix} \mathbf{i}_{dq} \quad (5)$$

Dealing with the first term, the current to flux relationship is (6), derived by coordinate transformation of the first three terms of (4):

$$\Delta\boldsymbol{\lambda}\hat{}_{dq} = \begin{vmatrix} \hat{L}_d & \hat{L}_{dq} \\ \hat{L}_{qd} & \hat{L}_q \end{vmatrix} \mathbf{i}_{dq} = \begin{vmatrix} L_0 + \frac{1}{2}L_2 - M_0 + M_2 & 0 \\ 0 & L_0 - \frac{1}{2}L_2 - M_0 - M_2 \end{vmatrix} \mathbf{i}_{dq} \quad (6)$$

where the inductances are indicated using the superscript "^". Equation (6) shows that the cross coupling terms of the inductances matrix are zero ($\hat{L}_{dq} = \hat{L}_{qd} = 0$) and the d- and q-axis inductances are not function of the motor position (see figure 5). Dealing with the fluxes produced by the unbalance of the mutual inductances ΔM_0, the fourth term of equation (4) becomes (7) when it is reported in the *dq* reference frame:

$$\Delta\boldsymbol{\lambda}\hat{\hat{}}_{dq} = \begin{vmatrix} \hat{\hat{L}}_d(\theta) & \hat{\hat{L}}_{dq}(\theta) \\ \hat{\hat{L}}_{qd}(\theta) & \hat{\hat{L}}_q(\theta) \end{vmatrix} \mathbf{i}_{dq} = -\frac{2}{3}\Delta M_0 \begin{vmatrix} 1+\cos\left(2\theta - \frac{2}{3}\pi\right) & -\sin\left(2\theta - \frac{2}{3}\pi\right) \\ -\sin\left(2\theta - \frac{2}{3}\pi\right) & 1-\cos\left(2\theta - \frac{2}{3}\pi\right) \end{vmatrix} \mathbf{i}_{dq} \quad (7)$$

where the inductances are indicated using the superscript "^^". In this case, the inductances in the *dq* reference frame vary with motor position and the cross coupling terms are not zero (see figure 6). Equation 6 demonstrates that the end-effect term ΔM_0 produces a cross-coupling term L_{dq} and also a variable contribution to the L_d and L_q terms as also evidenced in figure 3b. Figures 5 and 6 have been drawn using a simulation model developed in Matlab environment.

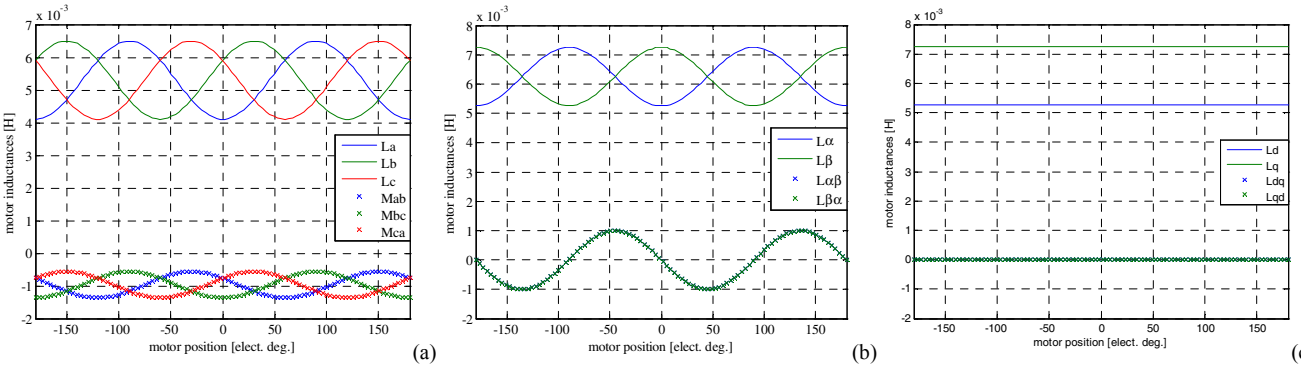

Fig. 5 Inductance waveforms obtained using the model (4) in the case of no end-effect ($\Delta M_0 = 0$), that means expression (6) in the *dq* frame: in the *ABC* (a), *α-β* (b) and *d-q* (c) reference frame.

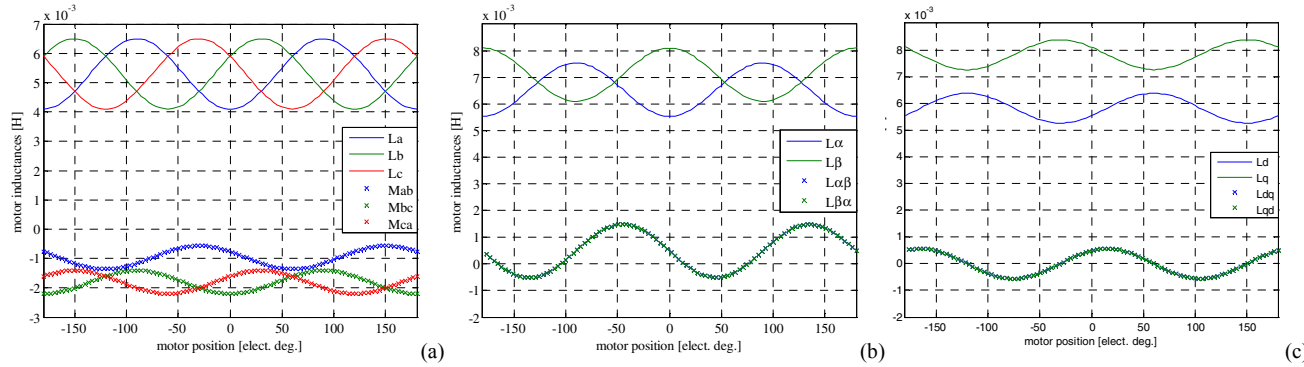

Fig. 6 Inductances waveform obtained using the model (4) including the end-effect effect ($\Delta M_0 \neq 0$), that means expression (5) in the *dq* frame: in the *ABC* (a), *α-β* (b) and *d-q* (c) reference frame.

IV. END-EFFECT COMPENSATION

As mentioned above, the *dq* inductances variable with the position and the cross coupling term produced by the end-effect cause stability problems to the sensorless control techniques based on magnetic saliency detection.

To overcome this problem, a compensation method has been derived according to the motor model previously determined. Using the complex notation [14] the inverse *d-q* magnetic model (5) can be written in the more compact form (8) where positive and negative sequence flux components are evidenced:

$$\mathbf{i}_{dq} = \left(\frac{L_d + L_q}{2\Delta}\right)\boldsymbol{\lambda}_{dq} - \left(\frac{L_d - L_q}{2\Delta} + j\frac{L_{dq}}{\Delta}\right)\boldsymbol{\lambda}^*_{dq} \tag{8}$$

where $\Delta = L_d L_q - L_{dq}^2$, $\lambda_{dq} = \lambda_d + j\lambda_q$ and $\boldsymbol{\lambda}^*_{dq} = \lambda_d - j\lambda_q$ is the negative sequence flux vector. The dependence of all the inductances on the motor position θ is implied for simplicity. Equation (8) can be rewritten using the estimated *d-q* reference frame, that leads the actual *d-q* frame by θ_{err} radians ($\mathbf{x}_{dq} = \mathbf{x}^{est}_{dq} e^{j\theta err}$, $\theta^{est} = \theta + \theta_{err}$) as defined in figure 7:

$$\mathbf{i}^{est}_{dq} = \left(\frac{L_d + L_q}{2\Delta}\right)\boldsymbol{\lambda}^{est}_{dq} - \left(\frac{L_d - L_q}{2\Delta} + j\frac{L_{dq}}{\Delta}\right)\boldsymbol{\lambda}^{est*}_{dq} e^{-j2\theta err} \tag{9}$$

The superscript '*est*' stands for the estimated *d-q* frame.

A. *End-effect error with pulsating voltage injection*

The most commonly adopted injection strategy is the pulsating voltage injection along the estimated *d*-axis. If this case is considered, the high frequency voltage (flux) along the estimated *q*-axis is zero. Therefore equation (9) can be rewritten under the assumption $\boldsymbol{\lambda}^{est}_{dq} = \boldsymbol{\lambda}^{est*}_{dq} = \lambda^{est}_{d}$, where $\lambda^{est}_{d} = \hat{V}_i / \omega_i$, $\hat{V}_i$ and ω_i are the injected voltage amplitude and frequency:

$$\begin{aligned}\mathbf{i}^{est}_{dq} = &\left[\left(\frac{L_d + L_q}{2\Delta} - \frac{L_d - L_q}{2\Delta}\cos(2\theta_{err}) - \frac{L_{dq}}{\Delta}\sin(2\theta_{err})\right) + \right.\\ &\left. + j\left(\frac{L_d - L_q}{2\Delta}\sin(2\theta_{err}) - \frac{L_{dq}}{\Delta}\cos(2\theta_{err})\right)\right]\lambda^{est}_{d} = \\ &= \mathbf{R}\lambda^{est}_{d}\end{aligned} \tag{10}$$

where $\mathbf{R}$ is a complex operator whose argument ψ is expressed in (11):

$$\psi = \arctan\left[\frac{(L_d - L_q)\sin(2\theta_{err}) - 2L_{dq}\cos(2\theta_{err})}{(L_d + L_q) - (L_d - L_q)\cos(2\theta_{err}) - 2L_{dq}\sin(2\theta_{err})}\right] \tag{11}$$

The angle ψ is the phase angle of the obtained high frequency current with respect to the injected flux vector. It must be noticed that ψ is function both of the position estimation error and the motor electrical position by means of the L_d, L_q and L_{dq} terms. Figure 8a reports the angle ψ as a function of the motor position for different values of the estimation error θ_{err}. For a given estimation error θ_{err}, the argument ψ varies with respect to the motor position and in particular the sign of ψ changes at different rotor positions. The red dashed curve in figure 8a demonstrates that with no estimation error the high frequency current is still not aligned with estimated *d*-axis. In other words, having zero-current along the estimated *q*-axis does not mean that the motor position is estimated correctly, as it usually happens with rotating machines. A proper compensation method is then necessary. When the estimation error is zero the phase between flux and current (11) becomes:

$$\psi_{LUT} = \arctan\left(-\frac{L_{dq}}{L_q}\right) \tag{12}$$

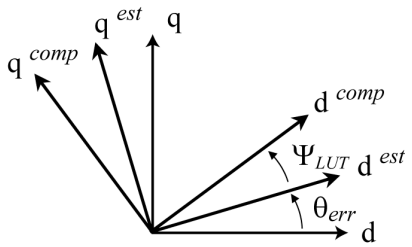

Fig. 7 – Definition of the various reference frames needed for sensorless control: motor *dq* axes, estimated axes (d^{est}-q^{est}), compensated axes (d^{comp}-q^{comp}).

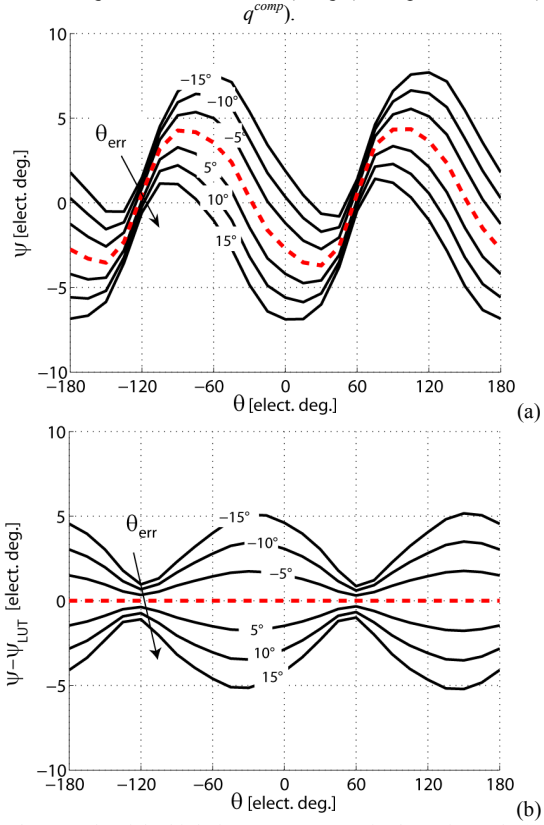

Fig. 8 Phase angle of the high-frequency current in the estimated (a) and in the compensated (b) *d-q* reference frames for several values of the position estimation error between -15 and +15 electrical degrees.

The angle ψ_{LUT} is the red dashed line plotted in figure 8a. It is convenient to represent the high frequency current in a compensated d-q reference frame that is shifted from the estimated dq reference frame by ψ_{LUT} radians as defined in figure 7. Considering $\mathbf{x}_{dq}^{comp} = \mathbf{x}_{dq}^{est} e^{-j\psi_{LUT}}$ and $\theta^{comp} = \theta^{est} + \psi_{LUT}$ gives:

$$\mathbf{i}_{dq}^{comp} = \mathbf{i}_{dq}^{est} e^{-j\psi_{LUT}} = |\mathbf{R}| \lambda_d^{est} e^{j(\psi - \psi_{LUT})} \quad (13)$$

The argument $\psi - \psi_{LUT}$, evidenced in (13), is reported in figure 8b for the same values of θ_{err} considered in figure 8a. In the compensated reference frame the sign of phase-angle of the high frequency current does not depend on motor position anymore. In particular, when the high frequency *q*-axis current in the compensated frame is zero, also the position error is zero and vice versa, as for standard position tracking methods. For this reason, the compensated *d-q* reference will be adopted for the demodulation of the position error information, as first proposed in [15] and represented in figure 10: the compensated reference frame is obtained, for any estimated position value, by means of a look-up table (LUT). In such reference frame the low-pass filtered product of i_d^{comp} and i_q^{comp} is proportional to the position estimation error [15].

The look up table values can be obtained using equation (12) in case the measured inductances are available, or using FEA simulations, or they can also be obtained in position sensored control, changing the compensation angle until the estimation error become negligible. In the latter case, the operation is repeated 56 times in different motor position covering 360 electrical degrees. To determine the LUT values, the experimental tests have been executed under no load and with 20 N external force, also to prove as the LUT values are not influenced by the motor load. The three LUTs (model, experiment no load and experiment with load) are reported in figure 9 and agree quite well. They have a peak value of about 4 electrical degrees and do not depend on motor load. It must be underlined the accurate results presented in figure 9 could be obtained very quickly by means of a two dimensional FEM analysis, since the tubular motor can be modeled in two dimensions with no error due to its axial symmetry.

V. Experimental Results

All the experimental investigations were performed using a dSPACE 1103 microcontroller board. The inverter switching frequency and the sample frequency of the control algorithm were set equal to 16 kHz, the inverter dead time is equal to 0.8 µs. The rated LPMSM parameters are as follows: current 2 A, Rs =9 Ω, polar pitch 56 mm (2π electrical radians), force constant 20 N/A, DC bus voltage 72 V. As said, the implemented sensorless strategy adopts a pulsating voltage signal injected along the estimated d-axis to detect the magnetic saliency. The implemented position observer scheme is reported in figure 10 [15]. During the experiments, the injected voltage signal had 12 V amplitude and 1 kHz frequency, generating 0.5 A phase currents.

The position step response under sensorless control has been tested with two different set points: 3 mm (19.3 electrical degrees) and 6 mm (38.6 electrical degrees), for evaluating the effectiveness of the proposed compensation technique. From figure 8a it is possible to notice that the angle ψ does not change its sign between -30 and +60 electrical degrees (if the estimation error is close to zero). In such position range a stable behavior of the sensorless scheme is expected also without the LUT. Outside the mentioned range the LUT is necessary to maintain a stable behavior: without the LUT the output of the low-pass filter would change its sign causing instability of the position observer.

Figure 11a shows the step responses (measured and estimated position) when a 3 mm position set point is applied and the compensation method is used, while in figure 11b are reported the same responses obtained without the LUT. In both cases the position does not exceeds 60 electrical degrees and the sensorless position control is stable.

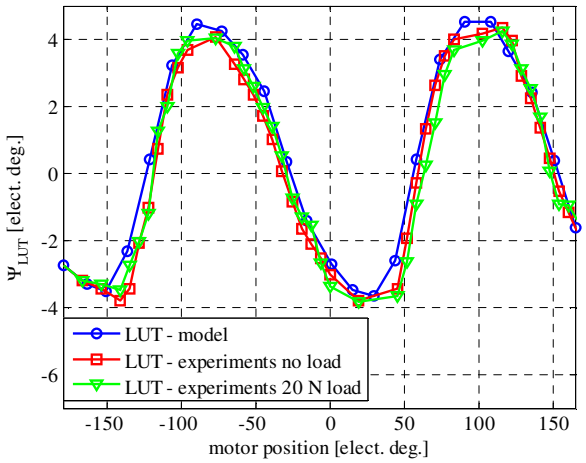

Fig. 9 Compensating LUT obtained using the mathematical model (blue circle), directly measured under sensorless control under no load conditions (red square) and with 40 N load (green triangle).

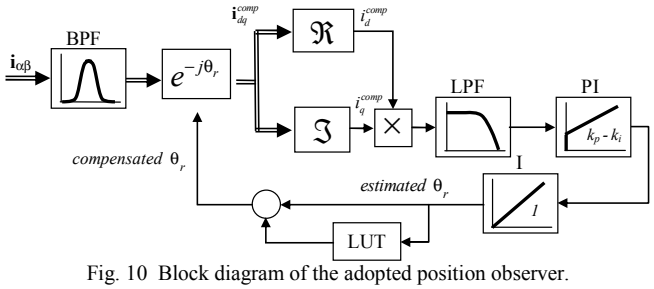

Fig. 10 Block diagram of the adopted position observer.

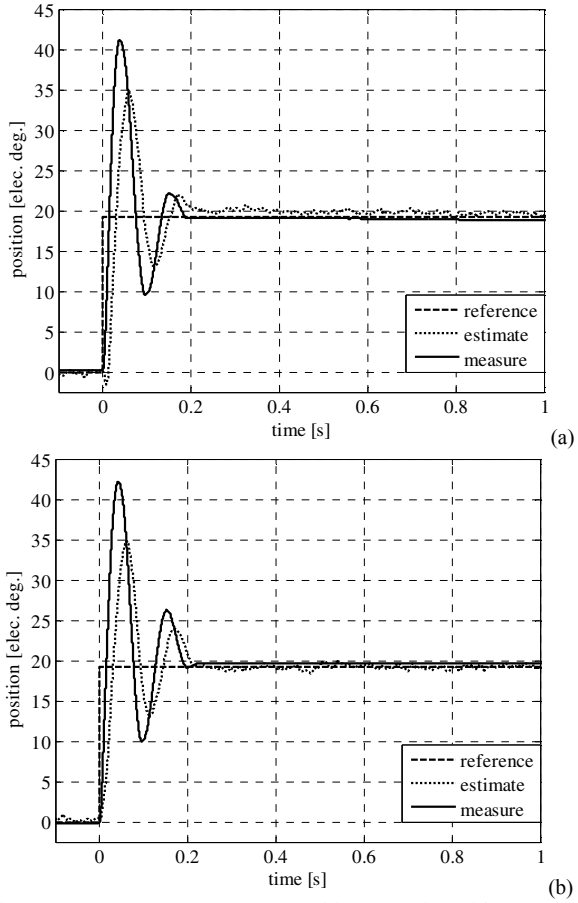

Fig. 11 Step response at 3 mm position set-point with LUT (a) and without LUT (b).

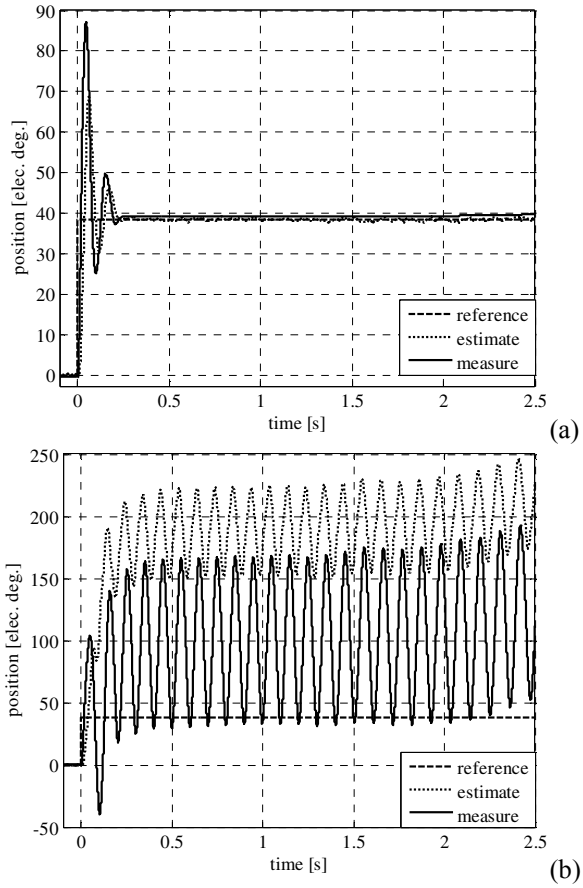

Fig. 12 Step response at 6 mm position set-point with LUT (a) and without LUT (b).

Figure 12 shows the response to a position step of 6 mm. If the LUT is adopted the control works properly (figure 12a). When the compensation method is disabled the control becomes instable as soon as the position exceeds 60 degrees, as shown in figure 12b. The tests shown in figures 11 and 12 prove that the LUT adoption is necessary to guarantee the stability of the sensorless position control.

It is important to note that the large position overshoot in the step response is due to the chosen position controller gains. In particular, an under-dumped position control loop allows to reduce position tracking error when a smoothed position reference is used in place of the step input. This is also demonstrated by the results obtained following a minimum time trajectory with maximum speed equal to 0.2 m/s and maximum acceleration equal to 1 m/s^2 that are reported in figure 13 in loaded conditions (20 N constant force was applied to the linear motor). The peak position estimation error is about 9 electrical degrees during transients (<1.4 mm) and falls always below 3 electrical degrees (<0.5 mm) at steady state. The results of figure 13 shown also as the estimation position fits well with real position.

VI. CONCLUSIONS

In this paper, the linear motor end effect has been analyzed and an accurate modelling procedure has been proposed. The introduced model has been used to compensate the unbalance among the mutual inductances caused by the end effect. In this way it is possible to avoid instability of the sensorless control schemes based on the detection of the magnetic saliency. The explained compensation method ensures good performances under any load, from zero to the rated, and also with severe control references, such as a step position reference.

REFERENCES

[1] Shujun Zhang, L. Norum and R. Nilssen, "Analysis of tubular linear permanent magnet motor for drilling application", International Conference on Electric Power and Energy Conversion Systems, 2009, pp1-5.

[2] X. Liu, Y. Ye, Z. Zheng and Q. Lu, "A novel tubular permanent magnet linear synchronous motor used for elevator door", International Conference on Electrical Machines and Systems, 2007. pp 801-804.

[3] N. Bianchi, "Analytical field computation of a tubular permanent-magnet linear motor", IEEE Transactions on Magnetics, vol. 36 , no. 5, September 2000, part 2.

[4] Jiabin Wang, Geraint W. Jewell, and David Howe, "A General Framework for the Analysis and Design of Tubular Linear Permanent Magnet Machines", IEEE Transactions on Magnetics, vol. 35, no. 3, May 1999, pp. 1986-2000.

[5] N. Bianchi, S. Bolognani, D. Dalla Corte, and F. Tonel, "Tubular linear permanent magnet motors: an overall comparison", IEEE Transactions

on Industry Applications, vol. 39, no. 2, March/April 2003, pp. 466-475.
[6] S.Y. Kim and I.J. Ha, "A new observer design method for HF signal injection sensorless Control of IPMSMs", IEEE Tran. Ind. Electron,, vol. 55, no. 6, June 2008, pp 2525-2529.
[7] C. Silva, G. M. Asher, and M. Summer, "Hybrid rotor position observer for wide speed-range sensorless PM motor drives including zero speed", IEEE Trans. Ind. Electron., vol. 53, no. 2, pp. 373-378, April 2006.
[8] Y. Jeong, R.D. Lorenz, T.M. Jahns, and S.K. Sul, "Initial rotor position estimation of an interior PM synchronous machine using carrier-frequency injection methods", IEEE Trans. Ind. Appl., vol. 41, no 1, pp. 38-45, Jan./Feb. 2005.
[9] R.C. Creppe, J.A. Covolan Ulson and J.F. Rodrigues, "Influence of Design Parameters on Linear Induction Motor End Effect", IEEE Transactions on Energy Conversion, vol. 23, no. 2, pp. 358-362, June 2008.
[10] Y.W. Zhu, S.G. Lee, K.S. Chung and Y.H. Cho, "Investigation of Auxiliary Poles Design Criteria on Reduction of End Effect of Detent Force for PMLSM", IEEE Transactions on Magnetics, vol. 45, no. 6, pp. 2863-2866, June 2009.
[11] H. Kim and R.D. Lorenz, "Carrier signal injection based sensorless control methods for IPM synchronous machine drives", Conference Record of the 2004 IEEE Industry Applications Conference, 2004. 39th IAS Annual Meeting. Vol. 2, 3-7 Oct. 2004 page(s):977 – 984.
[12] T. Matsuo and T.A. Lipo, "Rotor position detection scheme for synchronous reluctance motor based on current measurements", IEEE Transactions on Industry Applications, vol.31, no.4, pp.860-868, Jul/Aug 1995.
[13] I. Boldea and S. A. Nasar, "Linear motion electromagnetic devices", New York, Taylor & Francis, 2001.
[14] P. Guglielmi, M. Pastorelli and A. Vagati, "Cross saturation effects in IPM motors and related impact on zero-speed sensorless control", IEEE Trans. on Industry Applications, Vol. 42, Issue 6, Nov-Dec. 2006 Page(s):1516-1522.
[15] F. Cupertino, P. Giangrande, L. Salvatore, G. Pellegrino: "End effects in linear tubular motors and compensated position sensorless control based on pulsating voltage injection", accepted for publication on IEEE Transactions on Industrial Electronics, Digital Object Identifier: 10.1109/TIE.2010.2046577.

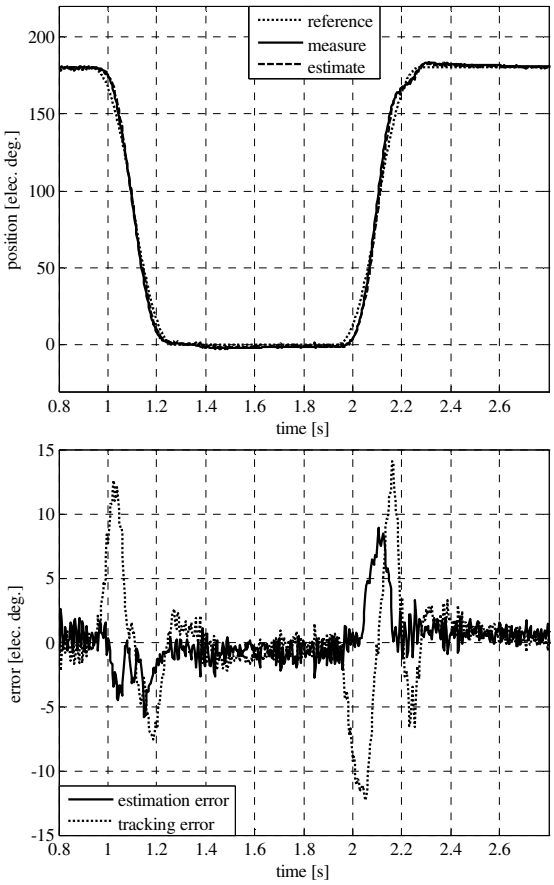

Fig. 13 Sensorless position control and errors performance under loaded conditions.